Article

Comparative Analysis of Estimated Small Wind Energy Using Different Probability Distributions in a Desert City in Northwestern México

Juan A. Burgos-Peñaloza [1] [iD], Alejandro A. Lambert-Arista [2,*] [iD], O. Rafael García-Cueto [1] [iD], Néstor Santillán-Soto [1] [iD], Edgar Valenzuela [2] [iD] and David E. Flores-Jiménez [1] [iD]

[1] Instituto de Ingeniería, Universidad Autónoma de Baja California, Mexicali 21280, Mexico; jburgospealoza@uabc.edu.mx (J.A.B.-P.); rafaelcueto@uabc.edu.mx (O.R.G.-C.); nsantillan@uabc.edu.mx (N.S.-S.); david.flores80@uabc.edu.mx (D.E.F.-J.)

[2] Facultad de Ingeniería, Universidad Autónoma de Baja California, Mexicali 21280, Mexico; evalenzuela.mondaca@uabc.edu.mx

[*] Correspondence: alambert@uabc.edu.mx

Abstract: In this paper, four probability functions are compared with the purpose of establishing a methodology to improve the accuracy of wind energy estimations in a desert city in Northwestern Mexico. Three time series of wind speed data corresponding to 2017, 2018, and 2019 were used for statistical modeling. These series were recorded with a sonic anemometer at a sampling frequency of 10 Hz. Analyses based on these data were performed at different stationarity periods (5, 30, 60, and 600 s). The estimation of the parameters characterizing the probability density functions (PDFs) was carried out using different methods; the statistical models were evaluated by the coefficient of determination and Nash–Sutcliffe efficiency coefficient, and their accuracy was estimated by the measured quadratic error, mean square error, mean absolute error, and mean absolute percentage error. Weibull, using the energy pattern factor method, and Gamma, using the Method of Moments, were the probability density functions that best described the statistical behavior of wind speed and were better at estimating the generated energy. We conclude that the proposed methodology will increase the confidence of both wind speed estimation and the energy supplied by small-scale wind installations.

Keywords: short-term wind variability; probability density function; small wind energy estimation

1. Introduction

The global climate emergency has given rise to great interest in the energy transition, which should contribute to mitigating CO_2 emissions caused by energy generation using conventional sources. Renewable energies play a significant role in this transition. It is necessary to estimate accurately the energy obtained from these sources to achieve this transition.

Global electricity demand decreased in 2020 but grew by 6% in 2021, representing one of the most significant annual growth rates since the 2010 monetary crisis [1]. Electricity consumption is expected to average 2.7% annual growth during the 2022–2024 period [1]. Considering the potential future demand, and the high costs of conventional energy resources and their environmental impact, the interest in using alternative energy sources has increased, further raising the need to evaluate the technical characteristics of these sources [2]. In the case of wind energy, estimations are made using a methodology based on medium-term average values (of the order of minutes) [3]. This methodology specifies a sampling frequency of 1 or 2 Hz to obtain mean velocities every 10 min. However, instantaneous wind speeds with a higher magnitude than the ten-minute average wind speed will not have the impact on the power calculated using the mean value that they

would if instantaneous power were calculated because power is directly proportional to the cube of the speed. Thus, the procedure underestimates power when using mean wind speed compared to the cumulative power of instantaneous wind speed values. In other words, the methodology minimizes wind variations in the order of seconds (short-term variability) and, consequently, wind power generation, which results in an underestimation of the wind resource [4].

Renewable energy has several advantages over fossil fuels, such as the availability of renewable resources to implement distributed generation systems, the access and modularity of its technologies, and the potential for each user to generate their own energy [5]. Therefore, wind energy is one of the most widely used renewable sources, and by 2021, it contributed with an installed capacity of 840 GW to the global electricity system [6]. Small wind energy (defined as wind energy that uses wind turbines with sweep areas of less than 200 m^2 [3]), or low-power wind energy, is a novel contribution to the electricity system, and the use of this technology is expected to increase complementing photovoltaic systems in distributed generation. As of the end of 2019, mini-wind power had an installed capacity of 1.72 GW worldwide [7]. Small wind installations have particular features, such as their capacity to provide energy in a distributed manner, feasible operation with moderate winds, requirement of small sites, and suitable integration in urban, semi-urban, industrial, and agricultural environments, and they are often used for the generation of energy close points [8].

Implementing wind energy requires accurate resource assessment [9,10], which can be achieved through a probability density function describing wind behavior. Typically, the Weibull probability density function can be used for this task. However, it is important to consider that other functions may better represent different wind regimes. According to Chang [11] and Cheng [12], the wind speed distribution for a particular location determines the available wind energy and the performance of an energy conversion system. Therefore, determining the function that best represents the wind regime at a location will contribute to a better estimation. Several studies have used different probability density functions, such as Weibull, Gamma, Raleigh, Beta, log-normal, and their combinations [11–29]. According to Wais [13,14], the two-parameter Weibull distribution is commonly used to model wind speed distribution in the wind industry. However, it may not always be sufficient for evaluating available wind energy. On the other hand, Wais suggests that the three-parameter Weibull distribution is advantageous because it fits better than the typical Weibull distribution with certain wind patterns. The literature also states that combined functions tend to have better statistical behavior compared to methods using a single function [19]. These combined distributions can be more efficient than single-function distributions for some wind regimes, although despite their advantages, the main drawbacks of combined distributions are their complexity and the computational time required in estimating the associated parameters [24]. In this regard, it is crucial to select the probability density function(s) appropriate to the data measured in the study area to obtain reliable energy estimations [9,11]; as stated by Cheng [12], the analysis must consider high-frequency wind data samples, i.e., short-term wind variability must be borne in mind.

Probability density functions are characterized by their statistical parameters of shape and scale, which can be obtained by different numerical methods; among the most used are the Maximum Likelihood Method (ML), Method of Moments (MM), Justus Empirical Method (EJ), Lysen Empirical Method (EL), Energy Pattern Method (EP), Graphical Method (GP), Standard Deviation Method (SD) and Modified Maximum Likelihood Method (MLM) [30]. Researchers use these methods to compare statistical model adjustment to measured data [30–39]. Using monthly data, Tizgui et al. [32] have found that EJ and MLM achieve a better estimation for the Weibull PDF, while Bilir et al. [19] consider EJ to be more accurate for annual estimation with hourly data and the Weibull PDF.

To evaluate the wind resource, the International Standard IEC-61-400-12-1 [3] establishes that wind potential estimates must be obtained using the ten-minute wind speed data, of average wind velocity recorded with a specific sampling frequency (e.g., 1 Hz) every

10 min. The averaging time, or stationarity period, defined as the time interval in which the wind velocity can be considered statistically constant, plays an important role in estimating wind potential. As the stationarity period increases, wind variability recorded in the time series decreases, negatively impacting the energy estimate. Rodriguez-Hernandez et al. [8] estimate an energy difference of 17% between stationarity periods of 1 and 10 min, while Arredondo et al. [4] find that the available energy density using 600 s (10 min) as the stationarity period results in underestimations of 1%, 8%, 10%, 13.7%, 19.4%, and 22.7% for stationarity periods of 300, 60, 30, 5, 1, and 0.1 s, respectively.

Consequently, improving the methodology for estimating wind energy considering short-term wind variability, the probability density function, and the appropriate method would help to increase the certainty of the energy that can be generated, thus contributing to the penetration of wind energy in the residential and commercial sectors. Therefore, this study aimed to determine the methodology that best estimates the energy obtained from a small wind turbine. This paper is structured as follows: Section 2 describes data collection and analysis, the determination of the probability density functions, the calculations for energy estimation and the statistical tests to validate such estimates. Section 3 presents the results obtained, and Section 4 presents the study's conclusions.

2. Methodology

The data used in this study were measured during 2017, 2018, and 2019 using a Campbell Scientific CSAT3 sonic anemometer, which records the orthogonal components u_x, u_y, and u_z of wind speed. The wind speed magnitude was obtained using the equation

$$v = \sqrt{u_x{}^2 + u_y{}^2} \tag{1}$$

where u_x and u_y are the easterly and northerly velocity components, respectively, and v is the velocity magnitude in the horizontal plane.

The anemometer can record at sampling frequencies from 1 to 100 Hz, with measurement errors of ± 8.0 cm/s and ± 4.0 cm/s in the horizontal and vertical components, respectively [40]. The instrument was placed 20 m above ground level at the UABC Engineering Institute in Mexicali B.C., which is geographically located at coordinates 32°37′52.32″ N and 115°26′40.48″ W. Mexicali's climate is classified as dry desert (BW), with extreme summer (average maximum temperature between 41 °C and 43 °C) and winter (average maximum temperature between 11 °C and 13 °C) temperatures. The average annual temperature is between 21 °C and 23 °C [41]. In 2022, the population of Mexicali was 1,049,792 residents [42], and its electricity consumption was 4736.29 GWh until 2016 [43]. A sampling frequency of 10 Hz was used in this study, thus obtaining 864,000 daily data equivalents to more than 3×10^8 data per year. From the original time series, time series of average values were obtained every 5 s, 30 s, 60 s and 600 s, which would be equivalent to recording the wind with those average sampling times.

2.1. Probability Density Functions and Methods for Statistical Parameter Estimation

Four different probability density functions (Weibull, Gamma, Rayleigh, and a combination of the three) were used to describe the data's statistical behavior. The PDFs take on a wide variety of shapes depending on the value of the shape parameter (α) and the level of stretch or squeeze indicated by the scale parameter (β). The (α) and (β) values for a dataset are unique, but there are diverse methods to determine them depending on the PDF used as explained in the following subsections.

2.1.1. Weibull Probability Density Function

The Weibull likelihood function was used to determine the characterization of the wind resource because it reliably describes wind behavior in different regions [27]:

$$f(v) = \frac{\alpha}{\beta} \left(\frac{v}{\beta}\right)^{\alpha-1} e^{-\left(\frac{v}{\beta}\right)^{\alpha}} \tag{2}$$

The two parameters, shape (α) and scale (β), were determined by the empirical methods of Justus, Lysen, and the energy pattern.

Empirical Justus Method (EJ)

In this method, parameters α and β are calculated using the following expressions

$$\alpha = \left(\frac{\sigma}{\bar{v}}\right)^{-1.086} \tag{3}$$

$$\beta = \frac{\bar{v}}{\Gamma(1 + \frac{1}{\alpha})} \tag{4}$$

where $\bar{v}$ is the mean wind speed and σ is the standard deviation, while Γ is the Gamma function [44].

Empirical Lysen Method (EL)

In this method, parameter α is calculated by means of Equation (3), while parameter β is calculated using the following expression [45]

$$\beta = \bar{v}(0.568 + \frac{0.433}{\alpha})^{\frac{-1}{\alpha}} \tag{5}$$

Energy Pattern Factor Method (E_{pf})

In this method, it is necessary to determine the energy pattern factor (E_{pf}) on which the shape factor depends; the equation is used for the scale factor. Factor E_{pf} is the ratio between the total power available in the wind and the power corresponding to the cube of the average wind speed [46,47]:

$$E_{pf} = \frac{\overline{v^3}}{\bar{v}^3} \tag{6}$$

$$\alpha = 1 + \frac{3.69}{(E_{pf})^2} \tag{7}$$

2.1.2. Rayleigh Probability Density Function

The Rayleigh probability density function is a special form of the Weibull distribution, in which the shape parameter always equals 2, and only the dispersion parameter (standard deviation) is used [23]:

$$f(v) = \frac{v}{\sigma^2}e^{-\frac{v^2}{2\sigma^2}} \tag{8}$$

2.1.3. Probability Density Function Gamma

The shape and scale parameters of the Gamma PDF are obtained using the methods of moments and maximum likelihood [48]:

$$f(v) = \frac{(\frac{v}{\beta})^{\alpha-1}e^{-\frac{v}{\beta}}}{\beta\Gamma(\alpha)} \tag{9}$$

Method of Moments (MM)

In the Method of Moments, the parameters are obtained as follows [48]:

$$\alpha = \frac{\bar{v}^2}{\sigma^2} \tag{10}$$

$$\beta = \frac{\sigma^2}{\bar{v}} \tag{11}$$

Maximum Likelihood Method (ML)

In this method, the parameters are obtained as follows:

$$\alpha = \frac{1 + \sqrt{1 + \frac{4D}{3}}}{4D} \tag{12}$$

$$\beta = \frac{\bar{v}}{\alpha} \tag{13}$$

where D is given by [48]

$$D = ln(\bar{v}) - \frac{1}{n}\sum_{i=1}^{n} ln(v_i) \tag{14}$$

2.1.4. PDF Mix

The PDF Mix was conceived as a function to describe the statistical behavior of the wind in each speed interval exactly, an objective that cannot be obtained with typical densities. From the Weibull, Gamma, and Rayleigh distributions obtained before, the PDF with the best performance is selected in each speed interval to achieve the goal. The distribution obtained is a continuous function by intervals.

2.2. Energy Estimation with PDF

The annual energy estimate for each year (2017, 2018 and 2019) and each time series (0.1, 5, 30, 60 and 600 s) were calculated using the PDFs and power curve of a wind turbine. The probability that the wind speed fell in the i-th interval [a, b] was calculated, first using the equation

$$p(a < \hat{v}_i < b) = F(v) = \int_a^b f(v)dv = F(b) - F(a) \tag{15}$$

where $f(v)$ is the PDF used, while a and b are the lower and upper bounds, respectively, of the i-th class of the velocity frequency histogram, $\hat{v}_i$ is the mean value of each class, and the function $F(v)$ is the cumulative probability function given by equation

$$F(v) = \int_0^v f(x)dx \tag{16}$$

It is necessary to point out that a and b belong to the set of natural numbers such that $b - a = 1$ is the histogram class size.

The interval probability found represents the percentage of the time, in the complete series, in which wind speed $\hat{v}_i$ occurred. This percentage is converted to hours (Δt) by multiplying it by the total number of hours in the time series.

As a second step, the power curve of the wind turbine was used to determine the power that, according to the manufacturer, the wind turbine delivers when the wind is flowing at speed $\hat{v}_i$. Then, the two previous values were multiplied (duration times power) to obtain the energy delivered by the small wind turbine with the wind flowing at wind speed $\hat{v}_i$. This procedure was repeated for each of the n intervals or classes. Finally, the estimation of the total energy generated per year E_w was obtained by summing the estimated energies in each speed interval as indicated by the equation

$$E_w = \sum_{i=1}^{n} P(\hat{v}_i)\Delta t \tag{17}$$

where $P(\hat{v}_i)$ is the power corresponding to the mean interval velocity.

Comparison between Estimated and Generated Energy

A 200 W small wind turbine was used hypothetically to evaluate the performance of the different statistical models in estimating energy. To compute the power based on wind

speed measurements obtained from the ultrasonic anemometer, we utilized the power curve provided by the manufacturer in the datasheet. The wind turbine can operate at slow wind speeds, starting from 1 m/s up until a survivor speed of 50 m/s. Typically, a power curve is only strictly valid for a subset of all atmospheric conditions, known as the inner range [49]. The outer range is the complementary subset of atmospheric conditions where wind turbines also operate. This uncertainty associated with wind spatial variability was not analyzed in this study.

The generated energy was obtained considering the instantaneous power corresponding to each of the m values of wind speed in each series using the following equation

$$E_r = \sum_{i=1}^{m} P(v_i)\Delta t_e \tag{18}$$

where Δt_e is the time corresponding to the stationarity period, and $P\ (v_i)$ is the instantaneous power delivered by the wind turbine when the wind has the speed v_i.

Energy comparisons were performed for each measured year and each stationarity period to determine which PDF resulted in a more accurate estimation compared to the energy produced by a wind turbine. The estimation error percentage was obtained from the expression [32]

$$\%E = \frac{E_r - E_w}{E_r} \times 100\% \tag{19}$$

2.3. Statistical Tests

The performance of the probabilistic models obtained was evaluated using the statistical tests described below, where y_i is the relative frequency of the observed velocity values, $\bar{y}$ is the mean relative frequency, and x_i is the expected frequency calculated with the theoretical distributions.

2.3.1. Coefficient of Determination (R^2)

The coefficient of determination is a measure of the relationship between a predicted probability density function and measured data. Mathematically, it is obtained as follows [50]:

$$R^2 = 1 - \left[\frac{\sum\limits_{i=1}^{n}(y_i - x_i)^2}{\sum\limits_{i=1}^{n}(y_i - \bar{y})^2} \right] \tag{20}$$

Its maximum value is 1, so the closer it is to 1, the better its fit.

2.3.2. Chi-Square (X^2)

The chi-square test is a simple and common goodness-of-fit test. It essentially compares a data histogram with the probability density function. The closer the result is to 0, the more accurate it is considered [32]:

$$X^2 = \sum_{i=1}^{n} \frac{(y_i - x_i)^2}{x_i} \tag{21}$$

2.3.3. Nash–Sutcliffe Efficiency Coefficient (NSEC)

The efficiency coefficient is another way to determine the accuracy of a prediction model; it is performed between the values of the probability density function and the

relative frequency of measured values. As with the R^2, the closer to 1, the more accurate the value is considered [51]:

$$NSEC = 1 - \frac{\sum\limits_{i=1}^{n}(x_i - \bar{y})^2}{\sum\limits_{i=1}^{n}(y_i - \bar{y})^2} \tag{22}$$

2.3.4. Root Mean Square Error (RMSE)

The root mean square error is an error that estimates the accuracy of the method by comparing the difference between the estimated values and the actual values. The closer the value is to zero, the more accurate the method [36]:

$$RMSE = \sqrt{\frac{1}{n}\sum_{i=1}^{n}(x_i - y_i)^2} \tag{23}$$

2.3.5. Mean Square Error (MSE)

The mean square error is a method that calculates the difference of the mean square error between the estimated values and the true value. As with the RMSE, the closer to zero the value, the more certain the result [36]:

$$MSE = \frac{1}{n}\sum_{i=1}^{n}(x_i - y_i)^2 \tag{24}$$

2.3.6. Mean Absolute Error (MAE)

The mean absolute error is an absolute test of the difference between two variables. It is the average of the absolute errors between the frequency of each PDF and the relative frequency of the measured data. The closer to zero, the better the result [36]:

$$MAE = \frac{1}{n}\sum_{i=1}^{n}\mid (x_i - y_i)^2 \mid \tag{25}$$

2.3.7. Mean Absolute Percentage Error (MAPE)

The mean absolute percent error is a relative measure that indicates the percentage error between the PDF and the relative frequency of the measured data. As with MAE, the lower the MAPE value, the more accurate the result [52]:

$$MAPE = \frac{1}{100}\sum_{i=1}^{n}\mid \frac{x_i - y_i}{y_i} \mid \tag{26}$$

3. Results and Discussion

The results of the behavior of the statistical parameters, statistical tests, and energy comparison behavior are described below.

3.1. Results of Statistical Parameters

Table 1 describes the annual data of the statistical parameters in the respective stationarity periods for each year analyzed; as can be observed, the average wind speeds are 2.09 m/s, 2.17 m/s, and 2.19 m/s, and they do not change in the different stationarity periods, which is consistent with the unbiased property of the mean of the sample means. On the contrary, the standard deviation decreases as the sample sizes (stationarity periods) increase, indicating that data dispersion around the mean decreases; that is, the wind velocity variability will become negligible as the stationarity period increases. Considering that the velocity dispersion is associated with the turbulent part of the flow, increasing the

period of stationarity represents a less turbulent and, therefore, less energetic flow. As can be seen, the highest values of the standard deviation correspond to the year 2019, which implies a larger data dispersion and may represent a higher amount of energy because it had a similar mean velocity to that of the other years.

Table 1. Statistical parameters for the different stationarity periods for 2017, 2018 and 2019.

	0.1 s		5 s		30 s		60 s		600 s		Year
	$\overline{v}$	σ	$\overline{v}$	σ	$\overline{v}$	σ	$\overline{v}$	σ	$\overline{v}$	σ	
	2.09	1.54	2.09	1.47	2.09	1.39	2.09	1.36	2.09	1.26	2017
	2.17	1.54	2.17	1.47	2.17	1.39	2.17	1.35	2.17	1.25	2018
	2.19	1.62	2.19	1.54	2.19	1.46	2.19	1.42	2.19	1.31	2019

Table 2 presents the shape (α) and scale (β) parameters defining the PDF for each year. The statistical parameters of the PDFs were determined using diverse methods. For the Weibull PDF, the *EJ*, *EL*, and E_{pf} methods were used, which resulted in the WEJ, WEL, and WE_{PF} distributions, respectively. The RSD distribution was obtained using the SD method with the Rayleigh PDF. For the Gamma PDF, the MM and ML methods were used to obtain the GMM and GML distributions, respectively. According to the shape and scale parameters equations in each method, there is an inversely proportional relationship between (α) and (σ) such that if the variability of the data decreases, the alpha parameter increases.

Table 2. Shape (α) and scale (β) parameters for the different stationarity periods for 2017, 2018 and 2019.

Method	0.1 s		5 s		30 s		60 s		600 s		Year
	α	β	α	β	α	β	α	β	α	β	
	1.367	2.304	1.463	2.309	1.550	2.325	1.593	2.331	1.729	2.346	2017
EJ	1.451	2.396	1.526	2.411	1.620	2.420	1.667	2.431	1.820	2.444	2018
	1.388	2.403	1.464	2.420	1.554	2.437	1.598	2.444	1.735	2.460	2019
	1.367	2.305	1.463	2.311	1.550	2.327	1.593	2.333	1.729	2.348	2017
EL	1.451	2.398	1.526	2.413	1.620	2.428	1.667	2.433	1.820	2.446	2018
	1.388	2.405	1.464	2.422	1.554	2.439	1.598	2.446	1.735	2.462	2019
	1.332	2.293	1.370	2.286	1.453	2.307	1.495	2.315	1.615	2.334	2017
E_{pf}	1.360	2.374	1.435	2.343	1.526	2.411	1.573	2.419	1.717	2.436	2018
	1.296	2.373	1.372	2.397	1.454	2.418	1.496	2.427	1.618	2.447	2019
	1.851	1.129	2.017	1.036	2.243	0.932	2.359	0.886	2.744	0.762	2017
MM	1.980	1.090	2.178	0.997	2.430	0.893	2.562	0.847	3.016	0.720	2018
	1.830	1.197	2.020	1.085	2.253	0.972	2.372	0.923	2.760	0.793	2019
	2.332	0.897	2.477	0.843	2.678	0.78	2.790	0.845	3.283	0.637	2017
ML	2.380	0.910	2.559	0.848	2.779	0.781	2.900	0.748	3.430	0.632	2018
	2.302	0.952	2.466	0.888	2.676	0.819	2.789	0.785	3.264	0.671	2019

Figure 1 shows the behavior of the shape and scale parameters for the analyzed period using each of the methods mentioned above. It can be observed that the behavior is similar for each parameter during the three years. The importance of the short-term wind variability considered in each stationarity period can also be observed as reported in other studies [4,8] because both parameters (α and β) present different values in the diverse periods. In fact, as we mentioned above, both parameters change their value, as the dispersion of the data decreases when the stationarity period increases. This results in a different function even using the same method as shown by the analysis performed by other authors using a single function with different methods [10,27]. The consequence

of this result is that the estimated energy in the different stationarity periods varies even when using the same PDF with a specific method as shown in the following subsection.

Another noteworthy aspect is that two of the five methods, MM and ML, are very sensitive to short-term variability. The graphic in Figure 1 illustrates the most significant variations in MM and ML observed across different stationarity periods. By referring to the data presented in Table 2, we can confirm that the errors for alpha and beta parameters with MM are approximately 50%, over the range of the stationarity periods shown. Therefore, using these methods to determine the statistical parameters of the densities could result in a more significant energy estimation error.
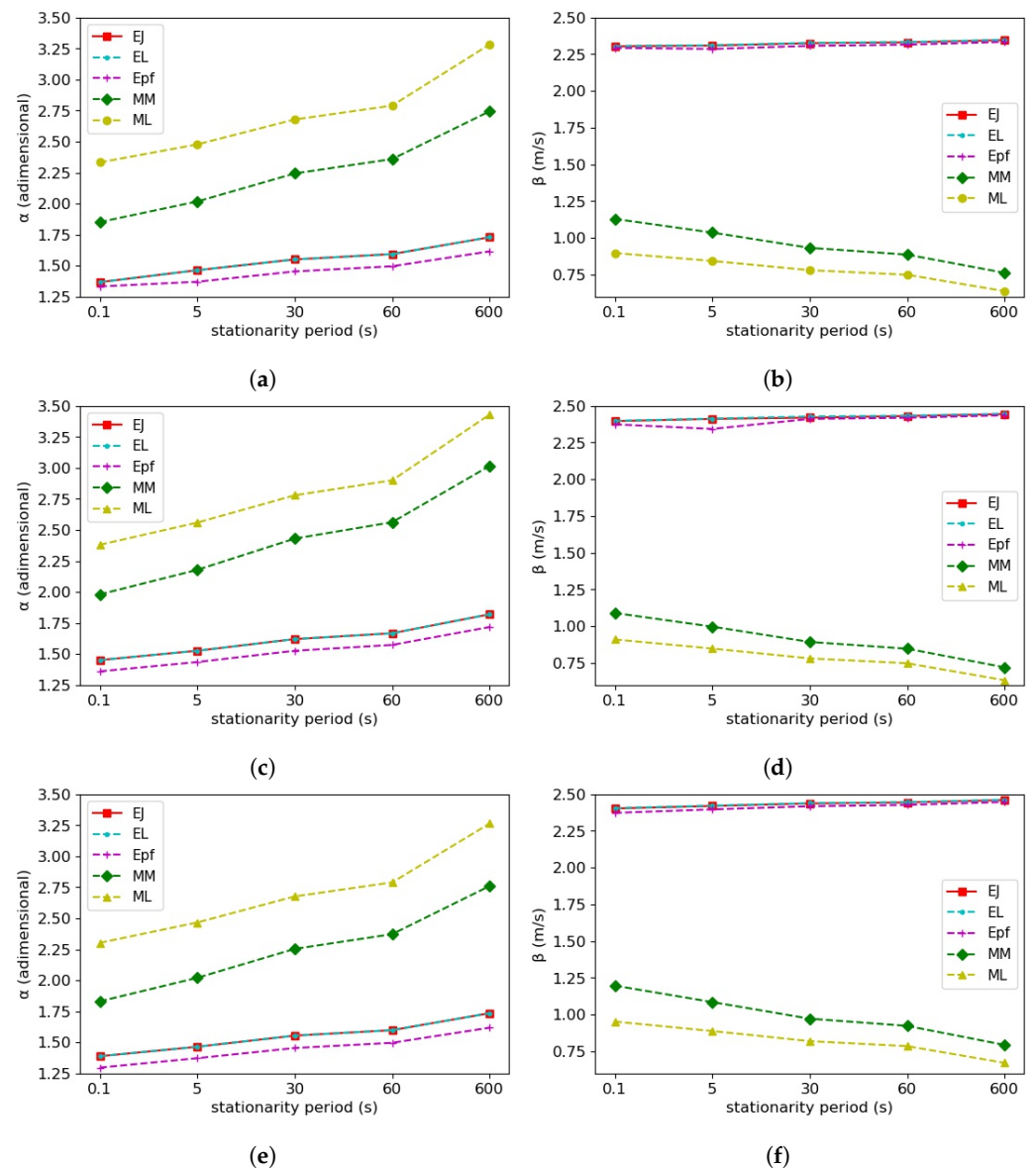
Figure 1. Shape and scale parameters. (**a**) Shape parameters for 2017. (**b**) Scale parameters for 2017. (**c**) Shape parameters for 2018. (**d**) Scale parameters for 2018. (**e**) Shape parameters for 2019. (**f**) Scale parameters for 2019.

Figure 2 shows two important aspects. First is the adjustment of each statistical model with the measured data for the stationarity periods of 5 and 600 s for the three years analyzed, and second, the performance of each model in each speed interval. As can be seen, the different methods are prone to overestimate or underestimate certain speed intervals. For example, Rayleigh has the best performance in the second class in the two stationarity

periods for the three years but overestimates in the first class and underestimates in the remaining one. On the contrary, GMM and GML have a good approximation in the upper classes (wind velocity $\geq 5\,\text{m/s}$) for the two stationarity periods and the three years, which can favor energy estimation when the highest velocities occur.
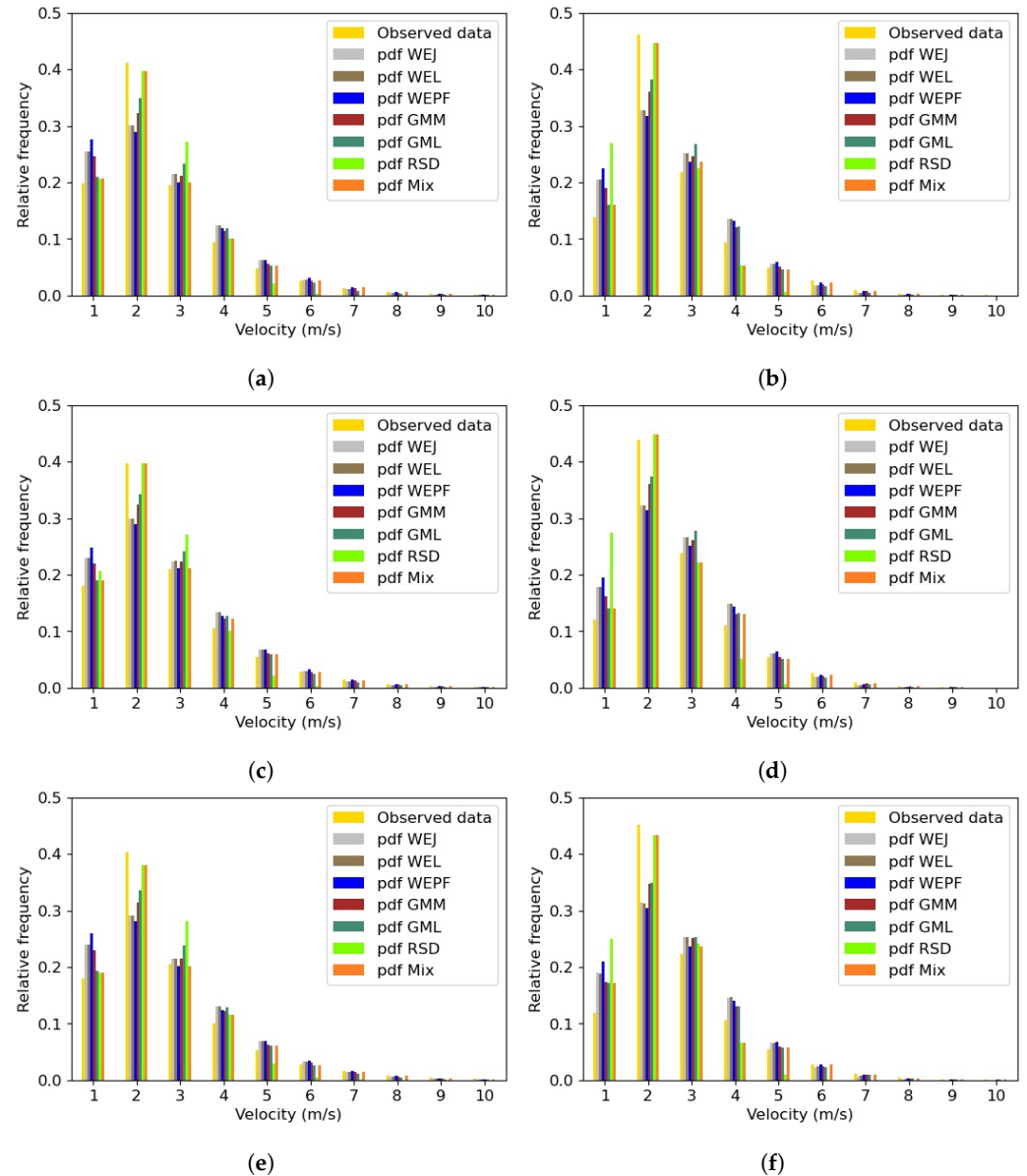
Figure 2. Comparison of relative frequencies with the stationarity periods indicated. (**a**) 5 s for 2017. (**b**) 600 s for 2017. (**c**) 5 s for 2018. (**d**) 600 s for 2018. (**e**) 5 s for 2019. (**f**) 600 s for 2019.

The distributions that best fit the measured data in each speed interval were selected for the construction of the PDF mix. For example, in Figure 2f, the best-fit density for the first class (0–1 m/s) is the GML function, for the second class (1–2 m/s) it is the RSD function, and for the third class (2–3 m/s) it is the WE_{pf} distribution. This procedure was followed for each stationarity period of every year.

3.2. Statistical Test Results

The parameters to estimate the goodness of fit between the observed and calculated data are presented in Tables 3 and 4 (5 s y 600 s, respectively) and the Appendix A. The results are grouped by stationarity period, indicating the method and year of the data series.

Table 3. Results of goodness-of-fit test/errors between observed and predicted data at 5 s.

Methods	R^2	NSEC	x^2	RMSE	MSE	MAE	MAPE	Year
PDF WEJ	0.92412	0.92114	0.07885	0.02767	0.00077	0.01091	66.8784	2017
	0.93596	0.93286	0.06714	0.02630	0.00069	0.01120	60.9770	2018
	0.91871	0.91540	0.08459	0.02757	0.00076	0.01054	66.9761	2019
PDF WEL	0.92408	0.92105	0.07895	0.02768	0.00077	0.01092	66.8227	2017
	0.93589	0.93274	0.06726	0.02632	0.00069	0.01120	60.9140	2018
	0.91866	0.91531	0.08469	0.02759	0.00076	0.01055	66.9149	2019
PDF WE_{pf}	0.90144	0.89913	0.10087	0.03129	0.00098	0.01141	56.1221	2017
	0.91746	0.91445	0.08555	0.02969	0.00088	0.01157	51.3477	2018
	0.89541	0.89281	0.10719	0.03104	0.00096	0.01113	56.4037	2019
PDF GMM	0.95177	0.94891	0.05109	0.02227	0.00050	0.00855	41.5378	2017
	0.96562	0.96299	0.03701	0.01953	0.00038	0.00806	34.7031	2018
	0.94893	0.94566	0.05434	0.02210	0.00049	0.00823	39.6690	2019
PDF GML	0.97245	0.97108	0.02892	0.01676	0.00028	0.00717	64.2016	2017
	0.97804	0.97704	0.02296	0.01538	0.00024	0.00711	54.8807	2018
	0.96951	0.96781	0.03219	0.01700	0.00029	0.00719	63.3709	2019
PDF RSD	0.97012	0.96475	0.03525	0.01850	0.00034	0.00818	81.5834	2017
	0.97664	0.96655	0.03345	0.01856	0.00034	0.00944	78.8445	2018
	0.96595	0.96090	0.03910	0.01875	0.00035	0.00889	82.1526	2019
PDF Mix	0.99849	0.99833	0.00167	0.00402	0.00016	0.00197	37.7363	2017
	0.99635	0.99602	0.00398	0.00641	0.00017	0.00268	36.1189	2018
	0.99593	0.99527	0.00473	0.00652	0.00004	0.00291	38.0726	2019

Table 4. Results of goodness-of-fit test/errors between observed and predicted data at 600 s.

Methods	R^2	NSEC	x^2	RMSE	MSE	MAE	MAPE	Year
PDF WEJ	0.88586	0.87805	0.12195	0.04604	0.00212	0.02483	55.1617	2017
	0.91137	0.90533	0.09467	0.03841	0.00148	0.02000	56.7452	2018
	0.87419	0.86513	0.13487	0.04742	0.00225	0.02535	53.4893	2019
PDF WEL	0.88583	0.87797	0.12203	0.04606	0.00212	0.02485	55.1464	2017
	0.91118	0.90507	0.09493	0.03846	0.00148	0.02002	56.6542	2018
	0.87401	0.86487	0.13513	0.04747	0.00225	0.02537	53.3943	2019
PDF WE_{pf}	0.86432	0.85520	0.14480	0.05017	0.00252	0.02527	44.2167	2017
	0.89855	0.89042	0.10958	0.04132	0.00171	0.02005	46.9639	2018
	0.85274	0.84197	0.15803	0.05134	0.00264	0.02541	42.8839	2019
PDF GMM	0.93902	0.93149	0.06855	0.03452	0.00119	0.01820	25.1186	2017
	0.96143	0.95665	0.04335	0.02599	0.00068	0.01319	28.4373	2018
	0.93223	0.92348	0.07652	0.03572	0.00128	0.01867	28.8496	2019
PDF GML	0.95445	0.95165	0.04835	0.02899	0.00084	0.01660	45.4149	2017
	0.96826	0.96670	0.03330	0.02278	0.00052	0.01256	38.2368	2018
	0.93372	0.92536	0.07464	0.03528	0.00124	0.01857	30.2912	2019
PDF RSD	0.91035	0.89512	0.10488	0.04270	0.00182	0.02312	77.6386	2017
	0.87896	0.84829	0.15171	0.04862	0.00236	0.02514	83.0592	2018
	0.90280	0.88828	0.11172	0.04316	0.00186	0.02489	78.4083	2019
PDF Mix	0.99323	0.99281	0.00719	0.01118	0.00013	0.00666	19.9490	2017
	0.99499	0.99430	0.00570	0.00942	0.00089	0.00552	24.4279	2018
	0.98198	0.97968	0.02033	0.01842	0.00034	0.01003	25.7630	2019

In general, all densities show good fits, highlighting the GMM and GML functions with the best fits in almost all the stationarity periods and years analyzed, while the RSD function presents the largest errors in the three years for all stationarity periods. Additionally, the dependence of the adjustment with the stationarity period is shown.

As can be seen in Tables 3 and 4, as the stationarity period increases, R^2 and NSEC decrease, and X^2 increases, and of the statistics that estimate the errors, RMSE, MSE, and MAE increase, while MAPE decreases. The above indicates that the best fit occurs with the shortest stationarity period.

On the other hand, per its definition, the goodness-of-fit tests and error statistics for the PDF Mix function corroborate its excellent performance. Thus, taking PDF Mix as a benchmark, we can identify bins where a specific density does not adjust properly or bins where it has a better performance.

3.3. Estimated vs. Generated Energy

Table 5 shows the amount of generated energy obtained from the power curve of the Aelos 200 W wind turbine [53], as well as the energy estimated by each of the PDFs with their different methods for the three years of study. As can be observed, the estimated energy decreases as the stationarity period increases because of decreased variability. For example, when using the Weibull PDF with the Justus method for the year 2017, differences of 1.9%, 4.3%, 5.4%, and 8.26% occur in the periods of 5, 30, 60, and 600 s, respectively, with respect to the period of 0.1 s. In the case of the Rayleigh PDF, the decreases are 5.5%, 12.6%, 15.1%, and 23.3%, while for the Gamma PDF in either of its two methods, energy differences of 1%, 2.2%, 3.1%, and 5.6%, approximately, can be observed. In the case of the PDF Mix function, decreases of 3%, 6.2%, 6.4%, and 14.9% can be observed. It is important to note that these decreases depend not on the methods used but on the short-term variability loss as indicated by the standard deviation values in Table 1, all of which result in a lower energy estimate.

Table 5. Generated and estimated energy (kWh) results for the different stationarity periods for 2017, 2018, and 2019.

	0.1 s	5 s	30 s	60 s	600 s	Year
Aeolos 200 W	227.11	227.11	227.11	227.11	227.11	2017
	177.93	177.93	177.93	177.93	177.93	2018
	267.73	267.73	267.73	267.73	267.73	2019
Method						
PDF WEJ	225	220.6	215.2	212.76	206.2	2017
	175.1	171	166.5	165.2	159.8	2018
	244.7	239	233	230.2	222.8	2019
PDF WEL	225.3	220.9	215.6	213.06	206.4	2017
	175.4	171.6	167.4	165.4	160	2018
	245.1	239.3	233.4	230.5	223.1	2019
PDF WE_{pf}	231.4	227	220.3	218.49	211.6	2017
	179.7	176.1	171.4	169.2	163.2	2018
	251.8	245.7	238.8	236.8	229.1	2019
PDF GMM	222.7	220.2	217.8	215.7	210.2	2017
	175.9	172.9	169.1	167.51	163	2018
	244.9	240.4	235	232.62	226.6	2019
PDF GML	215.9	213.5	210.7	209.4	204.5	2017
	169.9	167.6	165.2	163.8	159.4	2018
	234.5	231.5	227.9	225.88	220.2	2019
PDF RSD	172.9	163.3	151.1	146.7	132.5	2017
	129.4	121	112	107.7	97.2	2018
	188.2	174.5	161.5	155.6	140.9	2019
PDF Mix	229.6	222.69	215.2	214.7	195.3	2017
	178	172.6	169.5	167.8	166.1	2018
	252.4	241.3	232.8	230.33	218.7	2019

As indicated in Section 3.1, 2019 is the year with the most significant data dispersion. This is reflected in the energy values for that year, which were the highest for the energy computed with the wind turbine power curve and for the energy estimated with each of the seven statistical models used.

Table 6 shows the percentage error between the generated and estimated energy for each PDF, with its respective method, in the different stationarity periods and for each study year; the negative sign indicates an estimate greater than the generated energy. The table suggests that, based on percentage errors, the WE_{pf} PDF and the GMM PDF are associated with the smallest errors, making them more suitable for energy estimations. For example, for the year 2019, the GMM PDF has energy estimation percentage errors of 8.53, 10.21, 12.23, 13.11, and 15.36, while the WE_{pf} PDF presents a percentage errors of 5.95, 8.23, 10.81, 11.51, and 14.43 with respect to the generated energy, for each stationarity period. In addition, the PDF Mix could be considered because it has relatively small errors of 5.73, 9.87, 13.05, 13.97, and 18.31 with respect to the generated energy. Rayleigh PDF is the distribution with the highest error, which discards it as an adequate option for estimating energy in the study area.

Table 6. Energy estimation percentage error for the different stationarity periods for 2017, 2018, and 2019.

Methods vs. Aeolos 200 W	0.1 s	5 s	30 s	60 s	600 s	Year
	0.929	2.866	5.244	6.319	9.207	2017
PDF WEJ	1.591	3.895	6.424	7.154	10.19	2018
	8.602	10.73	12.97	14.02	16.78	2019
	0.797	2.736	5.068	6.186	9.119	2017
PDF WEL	1.422	3.558	5.918	7.042	10.08	2018
	8.453	10.62	12.82	13.91	16.67	2019
	−1.889	0.048	2.999	3.796	6.829	2017
PDF WE_{pf}	−0.995	1.028	3.670	4.4906	8.279	2018
	5.950	8.228	10.81	11.55	14.43	2019
	1.942	2.162	4.099	5.024	7.446	2017
PDF GMM	1.141	2.827	4.963	5.856	8.391	2018
	8.527	10.21	12.23	13.11	15.36	2019
	4.936	5.993	7.226	7.798	9.956	2017
PDF GML	4.513	5.806	7.154	7.941	10.41	2018
	12.41	13.53	14.88	15.63	17.75	2019
	23.87	28.10	33.47	35.41	41.66	2017
PDF RSD	27.27	32.00	37.05	39.47	45.37	2018
	29.71	34.82	39.68	41.88	47.37	2019
	−1.096	1.946	5.244	5.464	14.01	2017
PDF Mix	−0.039	2.996	4.738	5.693	6.649	2018
	5.726	9.872	13.05	13.97	18.31	2019

When comparing the error percentage of the energy estimates between the different statistical models in the same stationarity period, the differences can be an order of magnitude smaller than those obtained when comparing the error percentage of the energy estimates of the same PDF at different stationarity periods. For example, in the stationarity period of 600 s, the error percentage difference of the estimations between WE_{pf} and GMM for the year 2018 is 0.112 %, while the error percentage difference of the estimations between 600 and 5 s is 7.25 % for WE_{pf}, and 5.56 % for GMM. In general, it is shown that the error percentage difference between the estimations of the different statistical models in the same stationarity period is smaller than the error percentage difference of the estimations of a PDF in different stationarity periods. The above does not hold for the RSD function due to the large error percentage it presents.

4. Conclusions

This study used four probability density functions to estimate the energy that a small wind turbine installed for domestic use in a desert city in Northwest Mexico can generate. When the energy calculated from the wind turbine power curve was used as a reference, the results indicated that the accuracy of the energy estimates decreases as the stationarity period increases due to the short-term wind variability in the averaging process being neglected.

On the other hand, using different numerical methods to calculate shape and scale statistical parameters leads to different ways of the probability density functions, resulting in differences in estimated energy. In general, these differences are lower than those obtained when using a PDF in different stationarity periods. This means that the short-term temporal variability of the wind represents a higher uncertainty than that associated with the statistical models used in the energy estimate, except for the RSD function. However, the combined effect of both aspects causes the highest uncertainty.

Statistical modeling of the wind data showed that the globally most used distribution to describe the behavior of the wind, PDF WEJ, is not the best in the study area. Instead, the WE_{pf}, GMM, and Mix PDFs have, in general, lower errors, which is why they are considered better options for energy estimation in this region. The comparison between the estimated energy and the energy calculated from the wind turbine power curve confirm the above. Moreover, based on the analysis of the seven statistical models, we can infer that an inaccurate depiction of the statistical behavior of the data at high velocities leads to a severe underestimation of the energy, as is the case with the PDF RSD.

The above conclusion highlights the importance of selecting the probability density function and the numerical method a priori to determine the shape and scale parameters, to be used in the feasibility analysis of a small wind energy project.

In this regard, the use of the Weibull probability distribution as a probabilistic model and ten-minute data to estimate energy generation, established by the International Standard IEC61400-12-1 [3], leads to unreliable evaluations as a result of the underestimation of the resource [54]. This results in a lower penetration of small wind energy in locations such as Mexicali, where electricity consumption is above the national average due to its intense hot season. Therefore, increasing the reliability of energy estimates using small wind turbines will increase the viability of small wind energy projects due to greater certainty, promoting greater penetration of this renewable source, particularly in the residential and commercial sectors.

Abbreviations

The following abbreviations are used in this manuscript:

PDF	Probability Density Function
PDF W	Weibull Probability Density Function
EJ	Empirical Justus Method
EL	Empirical Lysen Method
E_{pf}	Energy Pattern Factor Method
E_w	Energy estimation
E_r	Actual energy
PDF R	Rayleigh Probability Density Function
PDF G	Gamma Probability Density Function
MM	Method of Moments
ML	Maximum Likelihood Method
PDF Mix	Mix Probability Density Function
R^2	Coefficient of Determination
x^2	Chi-Square
NSEC	Nash–Sutcliffe Efficiency Coefficient
RMSE	Root Mean Square Error
MSE	Mean Square Error
MAE	Mean Absolute Error
MAPE	Mean Absolute Percentage Error

Appendix A

Table A1. Results of goodness-of-fit test/errors between observed and predicted data at 0.1 s.

Methods	R^2	NSEC	x^2	RMSE	MSE	MAE	MAPE	Year
	0.92285	0.92036	0.07964	0.02710	0.00073	0.01041	66.4059	2017
PDF WEJ	0.93750	0.93506	0.06494	0.02380	0.00057	0.00917	65.5379	2018
	0.91842	0.91580	0.08420	0.02717	0.00074	0.01022	63.6357	2019
	0.92282	0.92029	0.07971	0.02712	0.00073	0.01041	66.3419	2017
PDF WEL	0.93750	0.93497	0.06503	0.02382	0.00057	0.00918	65.4738	2018
	0.91842	0.91573	0.08427	0.02718	0.00074	0.01023	63.5873	2019
	0.89940	0.89781	0.10219	0.03070	0.00094	0.01092	55.6649	2017
PDF WE_{pf}	0.91837	0.91636	0.08364	0.02701	0.00073	0.00968	57.0964	2018
	0.89130	0.88978	0.11022	0.03108	0.00097	0.01138	51.6974	2019
	0.94768	0.94500	0.05500	0.02252	0.00051	0.00858	39.3980	2017
PDF GMM	0.96301	0.96080	0.03921	0.01850	0.00034	0.00693	45.7116	2018
	0.94442	0.94177	0.05823	0.02259	0.00051	0.00828	42.1631	2019
	0.97249	0.97100	0.02899	0.01635	0.00027	0.00690	66.3538	2017
PDF GML	0.97858	0.97756	0.02244	0.01399	0.00020	0.00593	63.0985	2018
	0.97109	0.96942	0.03057	0.01637	0.00027	0.00696	64.3871	2019
	0.95583	0.95144	0.04857	0.02117	0.00045	0.00967	82.8553	2017
PDF RSD	0.96865	0.96134	0.03866	0.01837	0.00034	0.00797	81.8300	2018
	0.94752	0.94329	0.05671	0.02230	0.00050	0.01070	82.2250	2019
	0.99521	0.99351	0.00649	0.00774	0.00001	0.00338	33.8132	2017
PDF Mix	0.99779	0.92036	0.00234	0.00452	0.00000	0.00199	44.7972	2018
	0.99268	0.93506	0.01049	0.00959	0.00001	0.00412	38.8530	2019

Table A2. Results of goodness-of-fit test/errors between observed and predicted data at 30 s.

Methods	R^2	NSEC	x^2	RMSE	MSE	MAE	MAPE	Year
PDF WEJ	0.92201	0.91838	0.08162	0.03017	0.00091	0.01286	64.0270	2017
	0.93539	0.93203	0.06797	0.02794	0.00078	0.01266	59.3342	2018
	0.91267	0.90812	0.09188	0.03177	0.00101	0.01381	55.4190	2019
PDF WEL	0.92193	0.91825	0.08175	0.03020	0.00091	0.01286	63.9369	2017
	0.93498	0.93141	0.06858	0.02807	0.00079	0.01268	58.9407	2018
	0.91259	0.90798	0.09202	0.03179	0.00101	0.01382	55.3578	2019
PDF GMM	0.95480	0.95145	0.04855	0.02328	0.00165	0.00970	41.5393	2017
	0.96901	0.96634	0.03366	0.01966	0.00136	0.00868	25.9264	2018
	0.95009	0.94587	0.05413	0.02438	0.00059	0.01031	23.2579	2019
PDF WE$_{pf}$	0.90443	0.90092	0.09908	0.03325	0.00111	0.01329	54.4361	2017
	0.91966	0.91562	0.08438	0.03113	0.00097	0.01298	49.2061	2018
	0.89027	0.88594	0.114056	0.03539	0.00125	0.014216	54.5651	2019
PDF GML	0.97032	0.96896	0.03104	0.01861	0.00035	0.00841	56.1773	2017
	0.97728	0.97634	0.02366	0.01648	0.00027	0.00786	47.0188	2018
	0.96593	0.96401	0.035987	0.01988	0.00040	0.009364	47.6466	2019
PDF RSD	0.97273	0.96432	0.03568	0.01995	0.00040	0.01076	80.7793	2017
	0.96792	0.95220	0.04780	0.02343	0.00071	0.01800	79.7015	2018
	0.96740	0.95942	0.04058	0.02111	0.00045	0.01182	69.4238	2019
PDF Mix	0.99724	0.99719	0.00282	0.00561	0.00031	0.00278	31.3789	2017
	0.99903	0.99696	0.00303	0.00591	0.00046	0.00401	23.2060	2018
	0.99741	0.99727	0.00273	0.00548	0.00030	0.00266	18.8184	2019

Table A3. Results of goodness-of-fit test/errors between observed and predicted data at 60 s.

Methods	R^2	NSEC	x^2	RMSE	MSE	MAE	MAPE	Year
PDF WEJ	0.90673	0.89857	0.10143	0.03782	0.00143	0.01856	48.3084	2017
	0.93364	0.92991	0.07009	0.02923	0.00085	0.01371	58.2624	2018
	0.90966	0.90465	0.09535	0.03434	0.00118	0.01578	57.4877	2019
PDF WEL	0.90656	0.89833	0.10167	0.03787	0.00143	0.01858	48.2022	2017
	0.93352	0.92974	0.07026	0.02927	0.00086	0.01568	58.1640	2018
	0.90956	0.90449	0.09551	0.03437	0.00118	0.01805	57.4260	2019
PDF WE$_{pf}$	0.89074	0.88165	0.11835	0.04085	0.00167	0.01927	30.5040	2017
	0.91972	0.91512	0.08488	0.03217	0.00103	0.01387	48.4072	2018
	0.88848	0.88326	0.11674	0.03800	0.00144	0.01618	44.7211	2019
PDF GMM	0.95192	0.94767	0.05233	0.02717	0.00074	0.01323	25.1835	2017
	0.96457	0.95895	0.04105	0.02237	0.00050	0.00100	23.4617	2018
	0.94864	0.94693	0.05307	0.02562	0.00066	0.01149	40.9010	2019
PDF GML	0.95630	0.95391	0.04609	0.02550	0.00065	0.01288	40.3172	2017
	0.97684	0.97592	0.02408	0.01713	0.00029	0.00836	43.7285	2018
	0.96708	0.96599	0.03401	0.02051	0.00042	0.01031	41.1514	2019
PDF RSD	0.96603	0.95506	0.04494	0.02517	0.00063	0.01564	75.3075	2017
	0.95533	0.93529	0.06471	0.02809	0.00079	0.01614	80.1333	2018
	0.96145	0.95148	0.04852	0.02450	0.00060	0.01447	77.8835	2019
PDF Mix	0.99654	0.99625	0.00375	0.00727	0.00005	0.00390	16.7428	2017
	0.99899	0.99554	0.00446	0.00788	0.00006	0.00428	22.2970	2018
	0.99752	0.99740	0.00260	0.00567	0.00003	0.00299	29.6507	2019

References

1. International Energy Agency. Available online: https://www.iea.org/reports/electricity-market-report-january-2022/executive-summary (accessed on 22 April 2022).

2. Boroumandjazi, G.; Saidur, R.; Rismanchi, B.; Mekhilef, S. A review on the relation between the energy and exergy efficiency analysis and the technical characteristic of the renewable energy systems. *Renew. Sustain. Energy Rev.* **2008**, *16*, 3131–3135. [CrossRef]

3. International Standard IEC 61400-12-1. 2005. Available online: http://www.iec.ch/ (accessed on 14 October 2018).

4. Arredondo, M.G. Variabilidad a Corto Plazo de la Velocidad de Viento y su Efecto en la Estimación del Potencial Eólico. Master's Thesis, Instituto de Ingeniería UABC, Mexicali, México, 2 October 2018.

5. Burke, M.J.; Stephens, J.C. Political power and renewable energy futures: A critical review. *Energy Res. Soc. Sci.* **2018**, *35*, 78–93. [CrossRef]

6. World Wind Energy Association. Available online: https://wwindea.org/world-market-for-wind-power-saw-another-record-year-in-2021-973-gigawatt-of-new-capacity-added (accessed on 24 March 2022).

7. U.S Deparment of Energy. Office of Energy Efficiency and Renewable Energy: Distributed Wind Market Report. July 2018. Available online: https://www.energy.gov/eere/wind/articles/2018-distributed-wind-market-report (accessed on 7 May 2021).

8. Instituto para la Diversificación y Ahorro de la Energía. Available online: https://www.idae.es/tecnologias/energias-renovables/uso-electrico/eolica/eolica-de-pequena-potencia (accessed on 24 March 2022).

9. Rodriguez-Hernandez, O.; del Río, J.A.; Jaramillo, O.A. The importance of mean time in power resource assessment for small wind turbine applications. *Energy For. Sustain. Dev.* **2016**, *30*, 32–38. [CrossRef]

10. Rodriguez-Hernandez, O.; Martinez, M.; Lopez-Villalobos, C.; Garcia, H.; Campos-Amezcua, R. Techno-Economic Feasibility Study of Small Wind Turbines in the Valley of Mexico Metropolitan Area. *Energies* **2019**, *12*, 890. [CrossRef]

11. Chang, T.P. Estimation of wind energy potential using different probability density functions. *Appl. Energy* **2011**, *88*, 1848–1856. [CrossRef]

12. Cheng, K.-S.; Ho, C.-Y.; Teng, J.-H. Wind Characteristics in the Taiwan Strait: A Case Study of the First Offshore Wind Farm in Taiwan. *Energies* **2020**, *13*, 6492. [CrossRef]

13. Wais, P. A review of Weibull functions in wind sector. Renewable and Sustainable Energy Reviews. *Renew. Energy* **2017**, *70*, 1099–1107.

14. Wais, P. Two and three-parameter Weibull distribution in available wind power analysis. *Renew. Energy* **2017**, *103*, 15–29. [CrossRef]

15. Jaramillo, O.A.; Borja, M.A. Wind speed analysis in La Ventosa, Mexico: A bimodal probability distribution case. *Renew. Energy* **2004**, *29*, 1613–1630. [CrossRef]

16. Shoaib, M.; Siddiqui, I.; Amir, Y.M.; Rehman, S.U. Evaluation of wind power potential in Baburband (Pakistan) using Weibull distribution function. *Renew. Sustain. Energy Rev.* **2017**, *70*, 1343–1351. [CrossRef]

17. Jung, C.; Schindler, D. Global comparison of the goodness-of-fit of wind speed distributions. *Energy Convers. Manag.* **2017**, *133*, 216–234. [CrossRef]

18. Jung, C.; Schindler, D.; Laible, J.; Buchholz, A. Introducing a system of wind speed distributions for modeling properties of wind speed regimes around the world. *Renew. Energy* **2017**, *144*, 181–192. [CrossRef]

19. Datta, D.; Datta, D. Comparison of Weibull Distribution and Exponentiated Weibull Distribution Based Estimation of Mean and Variance of Wind Data. *Int. J. Energy Inf. Commun.* **2013**, *4*, 1–12.

20. Bilir, L.; Imir, M.; Devrim, Y.; Albostan, A. Seasonal and yearly wind speeddistribution and wind power density analysis based on Weibull distribution function. *Int. J. Hydrogen Energy* **2015**, *40*, 15301–15310. [CrossRef]

21. Hernandez-Escobedo, Q. Wind energy assessment for small urban communities in the Baja California Peninsula, Mexico *Energies* **2016**, *9*, 805. [CrossRef]

22. Dabbaghiyan, A.; Fazelpour, F.; Abnavi, M.D.; Rosen, M.A. Evaluation of wind energy potential in province of Bushehr, Iran *Renew. Sustain. Energy Rev.* **2016**, *55*, 455–466. [CrossRef]

23. Mohammadi, K.; Alavi, O.; McGowan, J.G. Use of Birnbaum-Saunders distribution for estimating wind speed and wind power probability distributions: A review. *Renew. Energy* **2017**, *143*, 109–122. [CrossRef]

24. Pishgar-Komleh, S.H.; Keyhani, A.; Sefeedpari, P. Wind speed and power density analysis based on Weibull and Rayleigh distributions (a case study: Firouzkooh county of Iran). *Renew. Sustain. Energy Rev.* **2015**, *42*, 313–322. [CrossRef]

25. Ouarda, T.B.M.J.; Charron, C.; Shin, J.Y.; Marpu, P.R.; Al-Mandoos, A.H.; Al-Tamimi, M.H.; Ghedira, H.; Al Hosary, T.N. Probability distributions of wind speed in the UAE. *Energy Convers. Manag.* **2015**, *93*, 414–434. [CrossRef]

26. Shu, Z.R.; Li, Q.S.; Chan, P.W. Statistical analysis of wind characteristics and wind energy potential in Hong Kong. *Energy Convers. Manag.* **2015**, *101*, 644–657. [CrossRef]

27. Kantar, Y.M.; Usta, I.; Arik, I.; Yenilmez, I. Wind speed analysis using the Extended Generalized Lindley Distribution. *Renew. Energy* **2018**, *118*, 1024–1030. [CrossRef]

28. Murthy, K.S.R.; Rahi, O.P. A comprehensive review of wind resource assessment. *Renew. Sustain. Energy Rev.* **2017**, *72*, 1320–1342. [CrossRef]

29. Teimourian, H.; Abubakar, M.; MYildiz, M.; Teimourian, A. A Comparative Study on Wind Energy Assessment Distribution Models: A Case Study on Weibull Distribution. *Energies* **2022**, *15*, 5684. [CrossRef]

30. Khan, J.K.; Uddin, Z.; Tanweer, I.S.; Ahmed, F.; Aijaz, A.; Jilani, S.U. Analysis of Wind Speed Distribution and comparison of five numerical methods for Estimating Weibull Parameters at Ormara, Pakistan. *Eur. Acad. Res.* **2015**, *II*, 14007–14015.

31. Carta, J.A.; Ramírez, P.; Velázquez, S. A review of wind speed probability distributions used in wind energy analysis. Case studies in the Canary Islands. *Renew. Sustain. Energy Rev.* **2009**, *13*, 933–955. [CrossRef]

32. Tizgui, I.; El Guezar, F.; Bouzahir, H.; Benaid, B. Comparison of methods inestimating Weibull parameters for wind energy applications. *Int. J. Energy Sect. Manag.* **2017**, *11*, 650–663. [CrossRef]

33. Usta, I. An innovative estimation method regarding Weibull parameters for wind energy applications. *Energy* **2016**, *106*, 301–314. [CrossRef]

34. Teyabeen, A.A.; Akkari, F.R.; Jwaid, A.E. Comparison of Seven Numerical Methods for Estimating Weibull Parameters for Wind Energy Applications. In Proceedings of the 2017 UKSim-AMSS 19th International Conference on Modelling and Simulation, Cambridge, UK, 5–7 April 2017; pp. 173–178.

35. Wang, J.; Hu, J.; Ma, K. Wind speed probability distribution estimation and wind energy assessment. *Renew. Sustain. Energy Rev.* **2016**, *60*, 881–899. [CrossRef]

36. Aukitino, T.; Khan, M.G.M.; Ahmed, M.R. Wind energy resource assessment for Kiribati with a comparison of different methods of determining Weibull parameters. *Renew. Energy* **2017**, *151*, 641–660. [CrossRef]

37. Indhumathy, D.; Seshaiah, C.V.; Sukkiramathi, K. Estimation of Weibull Parameters for Wind speed calculation at Kanyakumari in India. *Int. J. Innov. Res. Sci.* **2014**, *3*, 8340–8345.

38. Bukala, J.; Damaziak, K.; Kroszczynski, K.; Krzeszowiec, M.; Malachowski, J. Investigation of parameters influencing the efficiency of small wind turbines. *J. Wind Eng. Ind. Aerodyn.* **2015**, *146*, 29–38. [CrossRef]

39. Akgül, F.G.; Senotlu, B.; Arslan, T. An alternative distribution to Weibull for modeling the wind speed data: Inverse Weibull distribution. *Energy Convers. Manag.* **2016**, *114*, 234–240. [CrossRef]

40. Campbell Scientific, Inc. Manual CSAT3B Three-Dimensional Sonic Anemometer. 2015–2024. Available online: https://www.campbellsci.com/csat3b (accessed on 10 April 2024).

41. Secretaría de Protección al Ambiente de Baja California. Available online: https://www.gob.mx/cms/uploads/attachment/file/69289/12_ProAire_Mexicali.pdf (accessed on 5 December 2017).

42. Instituto Nacional de Estadística y Geografía. Available online: https://cuentame.inegi.org.mx/monografias/informacion/bc/poblacion/ (accessed on 4 November 2022).

43. Secretaría de Energía. Available online: https://www.gob.mx/sener/acciones-y-programas/estadisticas-del-sector-electrico-e-indicadores-de-cfe (accessed on 5 December 2017).

44. Justus, C.G.; Hargraves, W.R.; Mikhail, A.; Graber, D. Methods for estimating wind speed frequency distributions. *J. Appl. Meteorol.* **1978**, *17*, 350–353. [CrossRef]

45. Lysen, E.H. *Introduction to Wind Energy*, 2nd ed.; SWD Publication: Amersfoort, The Netherlands, 1983; CWD 82-1.

46. Akdağ, S.A.; Dinler, A. A new method to estimate Weibull parameters for wind energy applications. *Energy Convers. Manag.* **2009**, *50*, 1761–1766. [CrossRef]

47. Akdağ, S.A.; Guler, O. A novel energy pattern factor method for wind speed distribution parameter estimation. *Energy Convers. Manag.* **2015**, *106*, 1124–1133. [CrossRef]

48. Wilks, D.S. *Statistical Methos in the Atmospheric Sciences*, 2nd ed.; International Geophysics Series; Elsevier: London, UK, 2006; pp. 95–98.

49. Lee, J.C.Y.; Stuart, P.; Clifton, A.; Fields, M.J.; Perr-Sauer, J.; Williams, L.; Cameron, L.; Geer, T.; Housley, P. The Power Curve Working Group's assessment of wind turbine power performance prediction methods. *Wind. Energy Sci.* **2020**, *5*, 199–223. [CrossRef]

50. Baseer, M.A.; Meyer, J.P.; Rehman, S.; Alam, M.M. Wind power characteristics of seven data collection sites in Jubail, Saudi Arabia using Weibull parameters. *Renew. Energy* **2017**, *102*, 35–49. [CrossRef]

51. Nash, Sutcliffe. Pronóstico del caudal de los ríos a través de modelos conceptuales parte I—Una discusión de principios. *Revista Hidrología* **1970**, *10*, 282–290.

52. Mohammadi, K.; Alavi, O.; Mostafaeipour, A.; Goudarzi, N.; Jalilvand, M.W. Assessing different parameters estimation methods of Weibull distribution to compute wind power density. *Energy Convers. Manag.* **2016**, *108*, 322–335. [CrossRef]

53. Aeolos Wind Energy Ltd. Aeolos V Series. 2016. Available online: https://www.windturbinestar.com (accessed on 22 April 2016).

54. Rodriguez-Hernandez, O.; Jaramillo, O.A.; Andaverde, J.A.; del Río, J.A. Analysis about sampling, uncertainties and selection of a reliable probabilistic model of wind speed data used on resource assessment. *Renew. Energy* **2013**, *50*, 244–252. [CrossRef]